CTRC Research Publications

Cooling Technologies Research Center

2021

Comparative analysis of battery electric vehicle thermal management systems under long-range drive cycles

T.J. Shelly

J.A. Weibel

D. Ziviani

E.A. Groll

Comparative Analysis of Battery Electric Vehicle Thermal Management Systems under Long-Range Drive Cycles

Tyler J. Shelly[1,2], Justin A. Weibel[1], Davide Ziviani[1,2], Eckhard A. Groll[1,2]

[1]Cooling Technologies Research Center

School of Mechanical Engineering, Purdue University, West Lafayette, Indiana 47907 USA

[2]Ray W. Herrick Laboratories

School of Mechanical Engineering, Purdue University, West Lafayette, Indiana 47907 USA

Abstract

Due to increasing regulation on emissions and shifting consumer preferences, the wide adoption of battery electric vehicles (BEV) hinges on research and development of technologies that can extend system range. This can be accomplished either by increasing the battery size or via more efficient operation of the electrical and thermal systems. This study endeavours to accomplish the latter through comparative investigation of BEV integrated thermal management system (ITMS) performance across a range of ambient conditions (-20 °C to 40 °C), cabin setpoints (18 °C to 24 °C), and six different ITMS architectures. A dynamic ITMS modelling framework for a long-range electric vehicle is established with comprehensive sub models for the operation of the drive train, power electronics, battery, vapor compression cycle components, and cabin conditioning in a comprehensive transient thermal system modelling environment. A baseline thermal management system is studied using this modelling framework, as well as four common thermal management systems found in literature. This study is novel for its combination of comprehensive BEV characterization, broad parametric analysis, and the long range BEV that is studied. Additionally, a novel low-temperature waste heat recovery (LT WHR) system is proposed and has shown achieve up to a 15% range increase at low temperatures compared to the baseline system, through the reduction of the necessary cabin ventilation loading. While this system shows performance improvements, the regular WHR system offers the greatest benefit, a 13.5% increase in cold climate range, for long-range BEV drive cycles in terms of system range and transient response without the need for additional thermal system equipment.

Keywords: Battery Electric Vehicles, Integrated Thermal Management Systems, Equivalent Circuit Models, Heat Pump, Waste Heat Recovery

---

NOMENCLATURE

$C_1, ..., C_{10}$ AHRI Coefficients (-)

f Factor (-)

h Enthalpy

$\dot{m}$ Mass flow rate (kg/s)

N Compressor speed (Hz)

R   Recirculation ratio (%)

V Volumetric flow rate (m³/s)

$\dot{W}$ Compressor power consumption (kW)

Greek symbols

ρ Density (kg/m³)

Subscripts

amb Ambient condition

$cond$ Two-phase condensation properties

$data$ Mapped condition

$evap$ Two-phase evaporation properties

map Compressor map

$flow$ Flow rate

new Actual compressor condition

s   Isentropic

suc Suction

$total$ Total loading

$vent$ Ventilation loading

Acronyms

AHRI	Air-Conditioning, Heating, and Refrigeration Institute
APM	Auxiliary power modules
BEV	Battery electric vehicle
COP	Coefficient of performance
CSC	Constant speed cycle
DP	Dual polarization
ECM	Equivalent circuit model
EM	Electric motor or machine
ESS	Energy storage system
HEV	Hybrid electric vehicle
HFEDS	Highway fuel economy drive schedule
HVAC	Heating, ventilation, and air conditioning
HP	Heat pump
HWFET	Highway fuel economy test
HX	Heat exchanger
ICE	Internal combustion engine
IHX	Internal heat exchanger
ITMS	Integrated thermal management systems
MCT	Multi-cycle test
NEDC	New European driving cycle
PI	Proportional Integral
PTC	Positive temperature coefficient
PCM	Phase change material
SOC	State of charge
SOH	State of health
SP	Single polarization
TPIM	Traction power inverter modules

TXV   Thermostatic expansion valve

UDDS   Urban dynamometer drive schedule

VCC   Vapor compression cycle

WHR   Waste heat recovery

WLTP   Worldwide harmonised light vehicle test procedure

1. Introduction

As the vehicle fleet continues to electrify, the thermal management of battery electric vehicles (BEV) has significant effect on their operating range, especially in extreme climate conditions. Traditional heat sources available for cabin heating from internal combustion engines (ICE) are missing in BEVs, and furthermore, the replacement electrical components must adhere to tight thermal tolerances. The active management of these components is the focus of this study. Each component will be introduced in the context of its active thermal management strategy, impact on system range, and unique opportunities for integrated thermal management system (ITMS) architecture enhancements, followed by a review of recent literature that focuses on BEV thermal systems including the power electronics, cabin environment, battery conditions, and their optimization. Additionally, open-source battery modeling parameters available for ITMS modeling are reviewed.

Electric vehicle batteries and their associated cooling systems have been extensively studied in the literature, as previously exhaustively reviewed in Refs. [1] [2]. The goals of these past studies typically are to optimize existing cooling methods, establish alternate cooling methods, and investigate battery cell architectures.

BEV cooling methods investigated in the literature include air, liquid, direct refrigerant, immersion, and phase change cooling [1] [2] [3]. Air cooling ducts air either from the ambient

(passive) or conditioned from the cabin vapor compression cycle (VCC) (active) through the battery. This approach suffers from low cooling capacity due to the poor thermal conductivity of air and the size of the air ducts reduces the effective battery density, both contributing to a decreased range for the finalized system. Thus, air-cooled batteries are typically found in shorter range electric vehicles. Longer range BEVs typically implement liquid cooling due to more favorable heat transfer characteristics that allow for a denser cooling solution [4] [5] [6]. In the case of a direct liquid cooling solution, coolant is brought as close as possible to the battery for optimal heat transfer performance while an indirect solution places a cold plate along the bottom of the entire battery system's length while providing fins to interface with the battery. Further evolutions of direct liquid cooling, seeking improved heat transfer performance to ensure cell safety under extreme conditions, are two-phase direct refrigerant and immersion cooling concepts. Direct refrigerant systems bring two phase refrigerants to the battery via a cold plate and manifold system, like a direct liquid cooling solution, and evaporate the refrigerant. A more uniform and higher capacity cooling are associated with two-phase flow of the refrigerant across the battery cold plate. Passive two-phase immersion cooling submerges the BEV battery in dielectric fluid that boils in response to heat rejection from the battery. Currently, these two-phase cooling methods have limited implementation in the consumer market [1] [2]. The current study focuses on ITMS architectures having a secondary loop, indirect liquid cooling system for the battery. Analysis across a wide range of ambient conditions to examine their performance in heating and cooling modes has been identified as a gap in past research [1].

Heating, ventilation, and air conditioning (HVAC) solutions are critical for all vehicles to ensure consumer comfort across a wide range of ambient conditions. BEV cabin cooling solutions mirror those for ICE vehicles [7]. Typical cooling solutions include the use of a traditional VCC,

with potential improvements in cooling performance via suction to liquid-line heat exchangers, economization, flash tanks, or vapor injection cooling into modified compressor units. Suction to liquid-line heat exchangers ensures superheat at the compressor inlet while further subcooling the state outside of the condenser; performance enhancements depend upon the type of refrigerant and operating conditions. Economization splits the flow from the condenser and expands it to an intermediate temperature where it is used to further subcool the remaining flow and provide cooling between stages of compression. This reduces compressor losses while improving the evaporator performance due to the further subcooled liquid state but reduces the mass flow rate to the evaporator and thereby system capacity. A flash tank-based system operates on much the same principles of an economizer, with similar challenges as economization, namely, loss of evaporator capacity, addition of components, overall increase of system charge, and added complexity in control of the system [7].

The design of BEV cabin heating systems diverges from ICE vehicles. In ICE vehicles, the large amount of waste heat available from the engine can meet the heating needs of the vehicle even in extremely cold environments. Electric vehicles must rely on alternate forms of heating, such as direct electric heating from positive temperature coefficient (PTC) heaters, heat pumping, fuel-based heaters, or the use of recovered waste heat from the power electronics. Direct electric heating is intrinsically limited to coefficient of performance (COP) of 1, making it a large parasitic draw on the BEV traction battery. A heat pump (HP) reverses the flow inside of a typical VCC and rejects heat to the cabin while taking in heat from the ambient. HP heating systems typically suffer from a lack of heating capacity at extremely low ambient temperatures. Fuel heating sources burn an alternate dedicated heating fuel. While this approach overcomes the energy density issue and achieves the necessary heating capacity at extremely low-temperature ambient conditions, it

defeats the original purpose of electrification while increasing the operating costs of the vehicle. [7] Waste heat recovery (WHR) is the use of waste heat produced by the power electronics for either battery or cabin heating. This heating capacity is essentially free as otherwise it would be dissipated elsewhere in the vehicle mass or into the environment. Various combinations of these heating and cooling systems are investigated as alternate architectures defined later in the paper.

The last remaining components requiring thermal management in an BEV are the electric drive systems. These components typically include the auxiliary power module (APM), traction power inverter module (TPIM), and electric motor (EM) [8] [9], which are typically air or liquid cooled [10] [11].

Each of these individual BEV subsystems have been extensively investigated in the literature, whereas this current work focuses instead on the modeling of the entire ITMS for long-range BEVs. Within this narrowed scope, ITMS's of varying levels of complexity have been modeled in the literature. Yu et al. [12] established several different BEV HP architectures with the goal of finding a more efficient system. The studied architectures were a basic four-component HP system as a baseline, a secondary loop system, and a vapor injection system. Of these, the secondary loop system is proposed in this instance to enable the use of alternate refrigerants, such as R290 and R152a, which pose a risk to passenger safety if allowed to flow inside of the cabin environment. The authors concluded that the R290 secondary loop systems and R744-based traditional heat pump systems provide unique benefits for heating at extremely low ambient temperatures, but that a comprehensive analysis considering both heating and cooling demands was necessary as future work. Wang et al. [13] considered an R134a and R407C air-source HP in heating mode under a range of ambient temperatures from -15 °C to 0 °C. They found that the system can provide adequate heating performance down to an ambient temperature of -10 °C,

while experiencing a loss of capacity at -15 °C. This system was not characterized under moderate heating or cooling conditions, and further, did not consider the BEV thermal system demands beyond the cabin HVAC needs. Titov and Lustbader [8] comprehensively compared three thermal management systems: a basic HP system; HP and PTC; and HP, PTC, and WHR in the form of a combined fluid loop (CFL) system. Their analysis, while comprehensive in investigation of the heating cases, did not consider the cooling load or model the battery of the vehicle [8]. Tian et al. [14] analyzed an electric motor WHR system with a HP, the combined benefit of which was analyzed across differing heating and cooling cases that accounted for the different operating modes of the BEV thermal system. The system was simulated across a wide ambient temperature window of -7 °C to 43 °C. Only waste heat from the electric motor, rather than all the power electronics, was considered for recovery.

The final considerations for each the studied systems are the system capacity and drive cycle used. To establish and rate system performance under real-world driving conditions, representative drive cycles are used. One such cycle, NEDC, is used in Ref. [15] to establish appropriate boundary conditions for the performance of a cabin environment model which has an effective range of 6.84 miles (11 km). In Ref. [12], the WLRP cycle is used to compare different vehicle thermal system architectures across an effective range of 14.44 miles (23.24 km). In Ref. [8], the HWFET cycle is again used in a comparative study of thermal system architectures with an effective range of 10.26 miles (16.51 km), repeated twice. The trend is for shorter range BEVs to be studied under shorter range test cycles leaving a gap in long-range evaluation of BEV ITMSs.

The reviewed literature ranges in complexity, from single-cabin or cell models to complete coupled thermal management systems typically integrating up to two BEV thermal systems. While each of these studies provide insights into segments of specific BEV systems, the current study

aims to gain a holistic understanding across all relevant BEV systems. This is accomplished using a novel unified modeling framework that accounts for all BEV system thermal components, to allow for the comprehensive characterization, parametric study, and optimization for different BEV design goals. This holistic framework is then applied to long-range BEV's, a gap identified from the literature review, to examine any unique benefits which can be achieved with a variety of thermal management systems. To this end, the current work compares six different thermal system architectures, across a wide range of ambient temperatures from -20 °C to 40 °C, with consideration of the complete ITMS comprising the cabin, electronics, and battery. The systems are sized and compared for a high capacity BEV under a simulated Multi-Cycle Test (MCT) methodology, a long-range test not studied thoroughly in open literature. System performance is quantified based on the ultimate driving range across varying cabin setpoint conditions. The transient system response of the different flow management scenarios is also investigated.

2. Methodology

This section first introduces the baseline ITMS, governing assumptions, and boundary conditions. After, the dynamic modeling framework used to predict the performance of the ITMS for a full electric vehicle under a prescribed drive cycle, which was established in a previous study [11], is briefly summarized. The reader is directed to this previous work [11] for additional simulation details, relevant heat exchanger (HX) sizing, heat transfer correlations, power electronics assumptions, and drivetrain calculations. Specific updates made to the modelling framework compared to the past work are discussed in further detail; specifically, these updates extend the range of parameterization of the thermal system components and provide validation of the subcomponent models. Implications of the governing assumptions and models are discussed.

2.1 Baseline Thermal Management System

Our previous work [16] established a baseline TMS having the most typical solutions for cabin HVAC, battery thermal management, and electronics cooling for a long-range BEV. The baseline ITMS, detailed in Figure 2a, has a standard vapor compression cycle (VCC) that is used for direct cabin cooling and indirect battery cooling via a secondary water-glycol loop. Superheated R134a refrigerant is compressed across a parameterized scroll compressor and then condensed via heat exchange with ambient air. The refrigerant flow splits and can expand across two expansion valves. The first valve (V1) leads to the cabin heat exchanger (HX) while the second valve (V2) leads to the battery HX and cools a secondary water-glycol flow loop that conditions the battery through a cold plate attached to the battery. This secondary pumped loop has an electric heater to heat the battery to an appropriate setpoint in cold conditions, such as an event where the vehicle is cold soaked overnight. The system electronics are cooled through an additional pumped water-glycol loop which reject heat to the air via the radiator [16]. The final system function is the heating of the cabin and battery. Passenger comfort and safety are a function of heating performance, while the battery short-term capacity and long-term health are improved through proper thermoregulation. Cabin and battery heating are performed via heat sources interfaced with the water-glycol coolant flow for the battery and a secondary liquid-to-air heat exchanger for the cabin environment.

The two system radiators are sized from the overall dimensions of a commercially available radiator based on available engine compartment space, while the cabin and battery evaporator are sized via the e-NTU method to ensure a minimal footprint within the ducting of the EV's air system. The battery is sized to provide 100 kWh of capacity.

The system control logic follows typical component control schemes using proportional integral controllers. A variable-speed compressor is assumed to be electrically driven rather and controls for the inlet cabin air temperature across the cabin HX. System pumps and fans are controlled to set appropriate battery and cabin mean temperatures, respectively. The two expansions valves for the cabin and battery plate heat exchanger control the evaporator superheat and battery inlet temperature, respectively.

2.2 Dynamic Modeling Framework

The modeling approach is detailed here for each of the thermal, mechanical, and control volume systems in the previous section. The transient modeling framework is adopted in the Dymola modeling environment [17] and written in the Modelica language. This environment is multi-disciplinary, covering thermal, mechanical, electrical, and fluid flow systems with defined libraries of components. In this work, the TIL Suite is used to define thermal system components [18]. The modeling environment and specific details on each sub model are described in our previous work [16]. A summary is provided here, followed by further details pertaining to extension and verification of the model later in Section 2.2.

Beginning first with the drive train model, a force balance on a theoretical vehicle is constructed accounting for forces including rolling resistance, drag, and vehicle inertia. A number of key parameters such as mass of the system, drag, and rolling resistance coefficients, are assumed in the previous work [16], which then sets the total vehicle power requirements as a function of the input drive schedule. This then sets the power draw for the power electronics model.

The power electronics model is a black box model using singular constant efficiencies [16] to approximate both the power requirements experienced by each component and the total heat generation during a drive cycle. The power electronics include the EM, traction TPIM, and the APM. Each electronics component is parameterized as a heat source, adding heat to the liquid cooling loop defined in the baseline architecture via the TIL component libraries [18]. The final power demand of the traction power inverter module is the input to the battery model as an input variable, along with all other summed power demand in the system.

The battery pack is parameterized as a grouping of individual prismatic cells in line connected via defined series and parallel connections. The electrical side of the battery model is parameterized as an equivalent circuit model (ECM). To approximate the battery pack behavior, each module scales with electric circuit parameters according to the user-defined discretization. Further, on the thermal side, the batteries are taken considered as two-dimensional thermal models with user-defined parameters for conductivity and thermal capacity to match.

Open literature was surveyed to select the parameterized ECM for the battery. The findings of the literature review are summarized in Table 1. The studies reviewed were categorized based on several of important characteristics which indicate if the data can be utilized for the purposes of developing a battery ECM for transient thermal management investigations. These characteristics (the columns in Table 1) include the: cell geometry; equivalent circuit type (single polarization (SP) or dual polarization (DP)); whether the reported parameters are temperature-dependent, state of charge (SOC)-dependent, or state of health (SOH)-dependent; whether cell thermal properties such as thermal capacity, weight, or conductivity are provided; the parameterized temperature range; specified test conditions for replication and verification of the results of the paper; and finally, whether the necessary circuit parameters are reported. A priority

criterion for this survey was the desire to have a temperature range that extended down to -20 °C, an important extreme condition for evaluation of the ITMS architectures explored in this work. Of the models that cover such a temperature range [19] [20] [21], key parameters such as necessary cell geometry [19], upper temperature range [20], and cell thermal parameters [21] are missing to develop a complete ECM. For this reason, a cell parameterization with the complete information [22] but a narrower temperature range (40 °C to 5 °C) is adopted and used down to -20 °C by holding the resistance constant at low temperatures (5 °C to -20 °C). Conclusions for the open parameterization of battery data to enable more and more in-depth studies of BEV ITMS. With this the battery heat generation is established which then interfaces through the secondary loop architecture with the VCC.

Table 1: Review of parameterized battery equivalent circuit models

Cell Geometry	Model	Temperature Dependent	SOC Dependent	SOH	Cell Thermal Properties	Temperature Range	Test Conditions	Circuit Parameters	Source
Cylindrical	DP	No	Yes	NA	No	NA	Yes	Yes	[23]
NA	DP	No	Yes	NA	No	NA	Yes	Yes	[24]
NA	DP	Yes	Yes	NA	No	(45 °C to -5 °C)	Yes	NA	[25]
NA	SP	Yes	Yes	NA	No	(50 °C to 5 °C)	Yes	NA	[26]
Cylindrical	DP	Yes	No	NA	Yes	(40 °C to 10 °C)	Yes	Yes	[27]
Cylindrical	SP	Yes	Yes	NA	No	(40 °C to 0 °C)	Yes	Yes	[28]
Cylindrical	DP	Yes	Yes	NA	No	(45 °C to 15 °C)	Yes	Yes	[19]
NA	DP	No	Yes	NA	No	Yes	Yes	No	[29]
Prismatic	DP	Yes	Yes	NA	No	(45 °C to -5 °C)	Yes	No	[30]
Prismatic	DP	Yes	Yes	NA	No	(55 °C to 0 °C)	No	Yes	[31]
NA	DP	Yes (NA)	Yes	NA	No	No	Yes	No	[32]
NA	DP	Yes	Yes	Yes	No	(45 °C to 5 °C)	Yes	Yes	[33]
Prismatic	SP	yes	Yes	NA	Yes	(20 °C to -20 °C)	Yes	Yes	[20]
Pouch	NA	Yes	Yes	NA	No	(25 °C to -20 °C)	Yes	No	[21]
Prismatic	SP	Yes	Yes	NA	Yes	(40 °C to 5 °C)	Yes	Yes	[22]
Prismatic	R_{int}	No	Yes	NA	Yes	NA	Yes	Yes	[34]
Prismatic	SP	No	Yes	Yes	Yes	NA	Yes	Yes	[35]

Heat transfer calculations are calculated dynamically throughout the cycle run time by a set of heat transfer correlations implemented in heat exchanger models utilizing finite volume formulations. The correlations and heat exchanger sizes are summarized in the previous work. [16].

The compressor parameterization adopted in modeling the baseline system in our previous work assumed fixed isentropic, volumetric, and overall isentropic efficiencies [16]. This assumption, while common for preliminary component sizing, fails to capture key trends in compressor performance, namely, the decreased heating capacity of heat pumps at extremely low ambient temperatures on the order of -10 °C to -20 °C. To capture this key compressor trend over a wide range of ambient conditions AHRI mapping coefficients [36] were used to directly parameterize a compressor from a manufacturer.

$$\left(\dot{W}_{map}, \dot{m}_{map}\right) = C_1 + C_2 \cdot T_{evap} + C_3 \cdot T_{cond} + C_4 \cdot T_{evap}^2 + C_5 \cdot T_{evap} \cdot T_{cond} + C_6 \cdot T_{cond}^2 + C_7 \cdot T_{evap}^3 + C_8 \cdot T_{evap}^2 \cdot T_{cond} + C_9 \cdot T_{cond}^2 \cdot T_{evap} + C_{10} \cdot T_{cond}^3 \tag{10}$$

This approach has distinct advantages over alternative approaches. Firstly, the compressor can be sized to specific conditions for the cabin and battery system. Second, the compressor, and resulting compressor envelope, can be selected such that it covers the necessary operating conditions across a wide range of ambient temperatures. The compressor modeled in this study (Emerson ZS38K4E-PFV) is selected to provide a target capacity of 6 kW of cooling at an ambient temperature of 35 °C. This compressor speed is controlled with a proportional integral (PI)-controller based on an assumed maximum input taken from the compressor specifications.

$$\dot{m}_{comp} = \dot{m}_{map} \frac{N}{60} \tag{11}$$

$$\dot{W}_{comp} = \dot{W}_{map} \frac{N}{60} \tag{12}$$

The mapping adopted from the compressor manufacturer was constructed under a fixed superheat of 11.11 K which will not necessarily always be the case when simulating the system under transient operating conditions. These deviations are considered in the final governing equations for the compressor model by setting the factor f to 0.75 [37] in the following corrections:

$$\dot{m}_{new} = \dot{m}_{comp} \left(1 + f \cdot \left(\frac{\rho_{suc,new}}{\rho_{suc,data}} - 1 \right) \right) \tag{13}$$

$$\dot{W}_{new} = \dot{W}_{comp} \left(\frac{\dot{m}_{new}}{\dot{m}_{comp}} \cdot \frac{\Delta h_{s,new}}{\Delta h_{s,map}} \right) \tag{14}$$

It is further assumed that the compressor work is transferred to the refrigerant to fix the outlet state.

From the VCC, heat is extracted from the air recirculating from the cabin, mixing with fresh ventilated air from the ambient environment. The cabin environment is parameterized via inside and outside heat transfer coefficients which account for natural convection in the cabin environment and velocity driven airflow across the outside of the cabin. Solar and radiative fluxes are also parameterized to account for potentially changing weather conditions. Material parameters and orientations are also available for parameterization as well as the total internal air volume of the cabin.

It is important to verify that the cabin parameters considered in the model predict the imposed heat load within realistic expectations for a consumer long-range BEV. To verify the cabin model, predictions are compared to other literature solutions [12] [38] across three control variables: outdoor temperature, recirculation ratio, and solar flux. It is important to note that the cabin model parameters from the TIL libraries are kept as default and no specific cabin parameters from past literature sources have been adopted. This is done because past literature solutions offered incomplete data that would be required for a full parameterization, often neglecting to provide the cabin air volume, key dimensions, or materials and material properties. The comparison across the

stated control variables therefore aims to verify the magnitude and trend of the imposed cabin heat loading, rather than achieve an exact match with literature.

The verification of these loadings is completed for specific cases available from the original literature data, which typically characterize the total cabin heating load or decomposes the total into the ventilation and ambient loading. The input parameters for these simulations are shown in Table 2, which consider variations in the ambient temperature, recirculation ratio, and solar flux. Values in Table 2 are referenced where possible from the respective literature sources. In the case of solar flux variation, values for recirculation ratio were not available and instead were normalized against a third test point and held constant for the solar flux variation.

With variation of the ambient temperature, the bar chart in Figure 1a shows that the predicted steady state ventilation and ambient loads match well with the literature, capturing the trend of decreasing heat loads with increasing ambient temperature and matching the magnitudes. For the variation in recirculation ratio, shown in Figure 1b, the current simulations and literature data also agree, capturing both the magnitude and trend of the total heat load. Finally, the variation with solar flux is shown in Figure 1c, capturing both trends and magnitudes.

Table 2: Cabin validation simulation cases for variation in the ambient temperature, recirculation ratio, and solar flux.

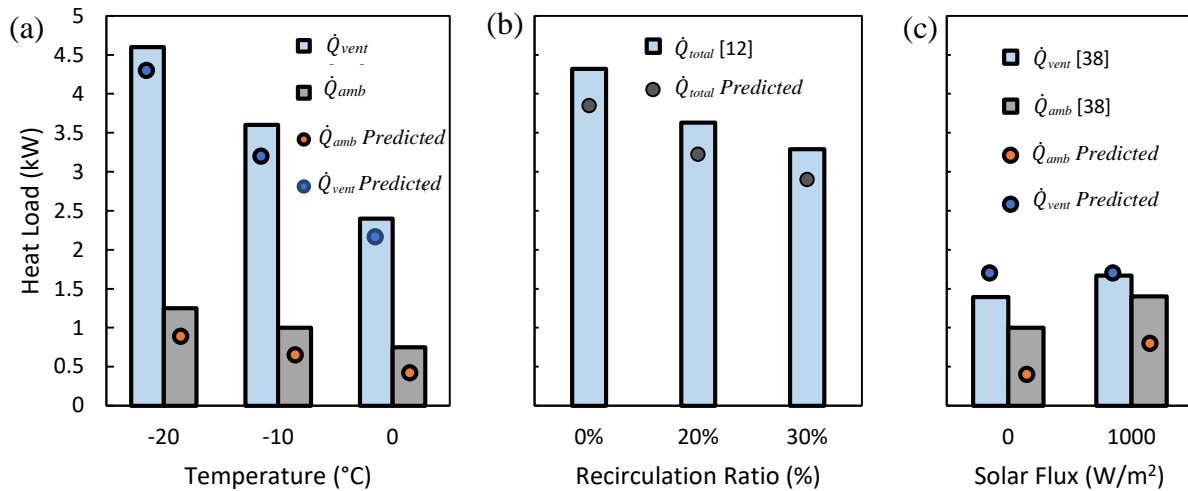| Cabin (°C)	Ambient (°C)	Solar Flux (W/m^2)	R (%)	V_{flow} (m^3/s)
		Ambient Temperature Variation		
24	0	NA	0%	0.07
24	-10	NA	0%	0.07
24	-20	NA	0%	0.07
		Recirculation Ratio Variation		
24	-10	NA	0%	0.07
24	-10	NA	20%	0.07
24	-10	NA	30%	0.07
		Solar Flux Variation		
22	43	0	30%	0.045
22	43	1000	30%	0.045

Figure 1: Comparison of the predicted cabin heat loads (dots) versus literature data (bars) for a variation in (a) ambient temperature, (b) recirculation ratio, and (c) solar flux. The heat load is either shown as the total ($\dot{Q}_{total}$), ventilation load ($\dot{Q}_{vent}$), or ambient load ($\dot{Q}_{amb}$).

3.   ITMS Architectures and Control

In addition to the baseline described above, five additional thermal management system architectures to be analyzed are described in the following subsections. Each of these architectures share similar thermal systems components with the baseline, with modifications that increase the complexity of the VCC or water-glycol flow control systems. Each system description that follows begins at the inlet to the compressor and continues around the various thermal management loops, highlighting key control logic and differences in the architecture.

3.1 Baseline with Low Temperature (LT) Radiator: "LT-HX"

The first additional system considered is the baseline system with the addition of a low-temperature radiator for battery cooling and an internal heat exchanger to the VCC, shown in Figure 2b. The proposed advantage of this system is the extension of system range through low-

temperature cooling of the battery. At low ambient temperatures when the cabin environment would not need to be cooled, while the battery may still need cooling after a long drive cycle to be to maintain it in its thermal limits. This system would allow for the VCC to be decoupled from battery cooling, thus saving overall energy. Additionally, the added internal heat exchanger would further subcool the condensed refrigerant exiting the radiator while ensuring compressor safety.

Starting at the inlet to the compressor, superheated vapor is compressed to a high temperature and then condensed across an ambient radiator until it exits in a subcooled condition. Here it enters the tube-in-tube internal heat exchanger where it is further subcooled by cold vapor leaving the evaporators. After expanding across a thermostatic expansion valve (TXV), the refrigerant diverts to either the cabin or battery evaporator. Exiting each evaporator, the two streams of vapor mix until they are further superheated as they pass through the cold side of the tube-in-tube heat exchanger to ensure compressor safety. In the secondary liquid cooling loop for the battery, beginning at the inlet to the battery cold plate, a water glycol mixture cools or heats the battery and enters a valve-controlled (V3) split in the flow. When the battery is hotter than the ambient, flow is directed to a front-end radiator for low-temperature heat rejection. When the battery is above its setpoint temperature or when it is below the ambient condition, the valve directs the coolant through the battery evaporator. The water glycol loops for the power electronics cooling and cabin heating remains unchanged from the baseline.

3.2 Heat Pump (HP): "HP"

A heat pump system (Figure 2c) is also considered to eliminate the need for the cabin PTC heater, as the heat pump operates at an inherently higher COP than the electric heater. From the inlet to the compressor, superheated vapor is compressed to a high-pressure state where it

encounters a four-way valve (V4) that is actuated based on the mode of the VCC system. For cabin cooling, the valve position is such that the VCC system operates identically to the baseline, where the front-end heat exchanger acts as a condenser and the cabin heat exchanger acts as an evaporator. For cabin heating, the refrigerant flow is reversed by the four-way valve. In this mode, the high pressure and temperature vapor exiting the compressor flows through the cabin heat exchanger, which now acts a condenser. During this heating mode of operation, the battery flow control valve (V2) is closed to prevent flow through this loop. Once the refrigerant condenses, it flows through the expansion valve (V1) and into the front-end radiator where it evaporates. The system diagram for the battery and power electronics cooling loops remains unchanged from the baseline system. The four-way valve is controlled such that it switches at a balance point of 21 °C ambient between heating and cooling modes. The balance point here is the point where conditioning demand switches from heating to cooling and vice versa based on ambient temperature.

3.3 Heat Pump and Positive Temperature Coefficient (PTC) Heater: "HP&PTC"

The next system considered is the heat pump system without elimination of the cabin PTC heater, shown in Figure 2d. The PTC heater can thereby compensate for capacity losses experienced by the heat pump at low ambient temperatures. The vapor compression systems remain unchanged from the heat pump diagram, but the cabin water-glycol heating loop from the baseline is added in tandem to the cabin heat exchanger to provide additional capacity during high-demand scenarios. The system control is modified from the baseline and heat pump systems to ensure that the HP, with an inherent COP greater than 1, is preferred to the electric heater for the cabin. This is illustrated when considering a typical cold soak heating scenario. Both the heat pump and electric heater are turned off initially. When the vehicle turns on, the heat pump responds with

a behavior according to its PI controller, eventually reaching a maximum RPM as it tries to heat up the cabin. If the heat pump remains maxed out for a specified wait time, then the electric heater engages and begins heating the cabin. During heating action, if any electric heating power above a threshold of 50 watts is being used, the compressor would remain at maximum capacity by default, letting the electric heater control the cabin inlet temperature. Once the high demand heat up period is finished, the electric heater would fall below the threshold value and the compressor would be controlled to set the cabin inlet temperature during steady operation. This control logic is maintained and expanded upon in the next two architectures and its implementation is referenced from Titov and Lustbader [8].

3.4 Heat Pump, PTC, and Waste Heat Recovery (WHR): "WHR"

The next system is a modification of the previous HP and PTC system presented in Section 3.3, with additional flow control that allows for the recovery of waste heat from the power electronics for the purposes of heating the battery or the cabin. The primary components that make up this system remain unchanged from the HP and PTC system, with only the addition of flow control valves that connect the power electronics water-glycol cooling loop to the cabin and battery water-glycol loop. Beginning at the inlet to the TPIM in Figure 2e, the water glycol cools each of the electronic components and exits to a four-way valve (V5). This valve can either place the power electronics loop in series with the secondary loop for battery heating, or maintain these as independent pumped loops. After either flowing through or bypassing the battery loop, the flow then passes to a second additional four-way valve (V6). This valve can similarly either place the power electronics in series with the cabin heating loop, or bypass this cabin loop. Together, these valves allow waste heat from the power electronics to supplement necessary heating for the battery (V5) or cabin (V6). Finally, after either bypassing or flowing through the cabin heat exchanger,

the water glycol flow comes to a simple bypass valve (V7) which plays a critical role in maintaining the temperatures of both the power electronics and the cabin environment. The valve operates to bypass the front-end radiator where the power electronics waste heat would typically be dumped to the environment if not being recovered.

Adding another potential heat source to control for the cabin inlet temperature in the architecture, in addition to the HP and cabin PTC, leads to three potential heat sources for controlling this variable at a given time. A layered control scheme is adopted from the CFL system investigated in the literature [8]. The control scheme considers the most efficient heat source as the waste heat recovered from the power electronics, followed by the heat pump, and finally the PTC heater. The control scheme works to use PTC power only when necessary during high demand periods. Once it falls below a threshold value of 50 watts, compressor speed is controlled to ensure cabin conditioning. Finally, once the compressor speed falls below a threshold value of 5 Hz, the bypass valve then works to ensure the cabin inlet temperature by proportionally bypassing flow from the exchanger in a range of 0% to 100%. Additionally, the bypass valve operates to ensure the temperature of the power electronics. If at any point during heating operation the power electronics go above a safety threshold of 120 °C, the bypass engages to cool the power electronics over a 5 min period. This bypass mode, while available, is not typically engaged as the partial bypass flow for cabin heating regulates that either waste heat is being directed to the cabin or the environment in periods of low heating demand. Regardless, with potentially three separate controllers available for a single bypass valve appropriate time constants and smoothing functions must be applied to eliminate local maxima and minima present during simulation. A time-averaged mean is applied to each mode-control variable as they are passed to the PI controllers for each component. These mode-control variables are the PTC power, compressor speed, and power

electronics temperature. Additionally, whereas modeling in the baseline system assumed the power electronics to be black-box efficiency models, parameterized thermal masses are added to the updated systems to ensure temperature fluctuations from the thermal system do not inadvertently trigger flow control logic. Finally, the remaining control logic governs actuation of the four-way valves that place the water glycol loops into series or bypass modes. For the battery flow control valve (V5), the control variable is the mean temperature of the battery; once heated to a lower temperature threshold of 15 °C, the four-way valve actuates to bypass the battery. This removes the heating load of the battery and increases the available waste heating capacity for the cabin. The cabin four-way flow control valve (V6) is actuated based upon the balance point temperature for system heating or cooling. In this way, whenever the ambient temperature is below the threshold of 20 °C waste heat is recovered to offset necessary electrical input.

3.5 Heat Pump, PTC, WHR, and Low-Temperature (LT) WHR: "LT-WHR"

The following novel system architecture operates much the same way as the previous system (Section 3.4), utilizing a combination of HP, PTC, WHR, but with the addition of low-temperature (LT) WHR. This architecture seeks to utilize the EV battery as another potential source of waste heat. Typical Li-ion batteries operate in a rather narrow band of temperatures from 15 °C to 35 °C, which does not offer a substantial temperature difference for meaningful recovery considering cabin setpoints from 18 °C to 24 °C. There is however a potentially larger temperature difference available for heat exchange with incoming fresh air that is necessary to prevent fogging, especially during extremely low ambient conditions, which could offer a meaningful opportunity for LT WHR. This is achieved in the system (Figure 2f), via an additional air to water-glycol heat exchanger in the battery secondary loop, which would be ducted with fresh air to extract waste heat from the battery once within its safe operating temperature range. Additionally, a final bypass

valve (V8) is added to route coolant through the appropriate heat exchanger based upon mode selection. These modes are determined by the operating temperature limits of the battery; the four-way valve (V4) is switched first to take the battery secondary loop out of series with the power electronics. Then, after a 100s wait period, the battery coolant is directed through the LT HX and conditions the incoming fresh air into the system.

3.6 Summary of Control Variables and Targets

All the control logic for each system is summarized in Table 3. Across heating and cooling cycles the systems actively control for battery mean temperature, battery inlet temperature, cabin mean temperature, and cabin inlet temperature.

Table 3: Independent and dependent control variables for thermal system components

Component	Architecture	Control Variable	Value	Dependent Variable
V1	All	Cabin Evaporator Superheat	5 °C	Evaporator Cooling Capacity
V2	All	Battery Inlet Temperature	User Chosen	Battery HX Capacity
V3	LT-HX	Battery Mean Temperature	User Chosen	Battery Flow Direction
V4	HP, HP&PTC, WHR, LT-WHR	Ambient Temperature	21 °C	VCC Flow Direction
V5	WHR, LT-WHR	Battery Mean Temperature	15 °C	Battery WHR Flow Control
V6	WHR, LT-WHR	Ambient Temperature	21 °C	Cabin WHR Flow Control
V7	WHR, LT-WHR	Electronics Temperature	120 °C	Electronics Flow Control

V8	LT-WHR	Battery Mean Temperature	15 °C	Battery LT-WHR Flow Control
C1	All	Cabin Inlet Temperature	User Chosen	VCC System Capacity
P1	All	None		Electronics Mass flow
P2	All	None		Cabin heater Mass flow
P3	All	Battery Mean Temperature	User Chosen	Battery Coolant Mass flow
F1	All	None		VCC Radiator Volume flow
F2	All	Cabin mean Temperature	User Chosen	Cabin air Volume flow
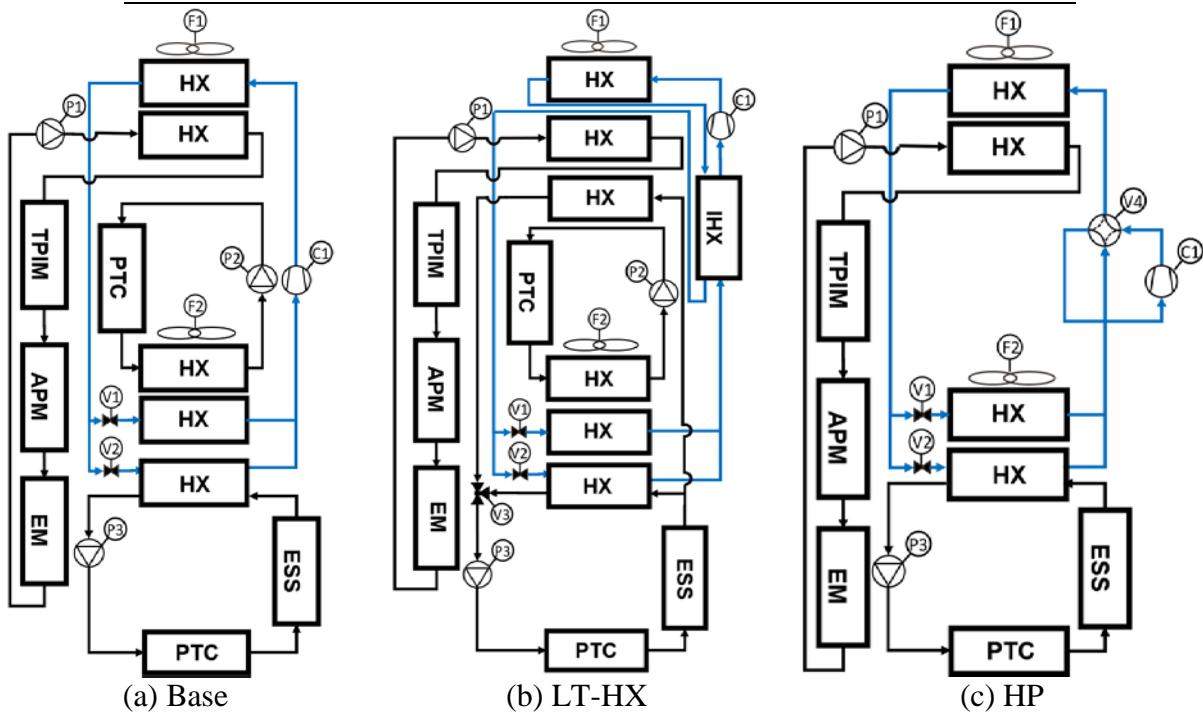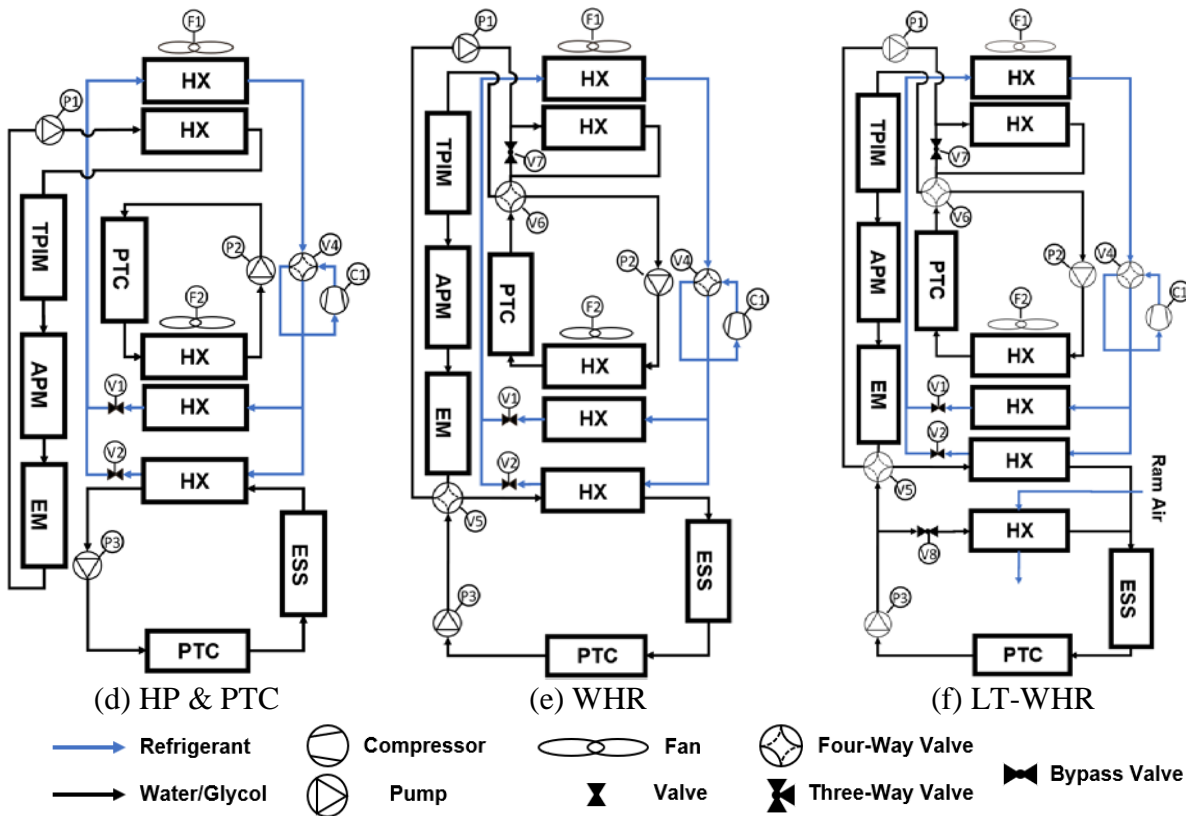
(a) Base   (b) LT-HX   (c) HP

Figure 2: Schematic flow diagrams of all battery electric vehicle (BEV) integrated thermal management system (ITMS) architectures: (a) Baseline (Base), (b) Baseline with low-temperature radiator (LT-HX), (c) Heat pump (HP), (d) Heat pump and PTC heater (HP&PTC), (e) Heat pump, PTC, and waste heat recovery (WHR), and (f) Heat pump, PTC, WHR, and low-temperature WHR (LT-WHR).

4. Simulation Conditions and Cases

This section outlines the critical boundary and initialization conditions, including boundary conditions for the ambient and vehicle velocity. The transient initialization strategy is discussed in the context of system charge, pressure initialization, PI control initialization, and the initialization of the system as it transitions between heating and cooling mode. Finally, the simulation test cases to be examined across the different ITMS architectures are outlined.

4.1 Boundary conditions

Ambient conditions can be provided either at various times of a parameterized day (including the precipitation, wind speed and direction, and changing sun condition and position) or under fixed conditions held constant throughout the simulation. For the purposes of this study, fixed conditions are assumed with the vehicle driving north with no wind on a clear sunny day, at constant ambient temperature, humidity, and the resulting air psychrometric properties. The vehicles cabin is exposed to direct and diffuse solar radiation of 600 and 200 W/m^2, respectively. The constant ambient temperature is varied parametrically between each case across a range of -20 °C to 40 °C.

The vehicles velocity schedule is defined by the time varying input of a multi-cycle test (MCT) [39] methodology, as described in detail in the preceding work [16]. In practice, this cycle is designed to avoid long dynamometer schedules experienced when testing the ranges of long range EV's. Under previous testing schemes classic rating cycles such as HWFET and UDDS drive schedules would need to be repeated tens of times to fully deplete the EV battery and reach end of test condition. The MCT methodology is designed to examine high and low charge dynamics while shortening overall testing time via high constant speed cycles which drain the battery quickly. This provides benefit for simulation time as well leading to shortened simulation time overall.

4.2 Initialization conditions

As the model is transient in nature, initialization conditions must be specified to pose the problem to be solved by the numerically. The initial conditions include pressure and temperature initialization for the VCC equipment and fluid, temperature initialization conditions for solid

thermal masses in the system, and initial temperature for the cabin volume. For the VCC, low- and high-side pressures of the compressor are initialized at 500 kPa and 1200 kPa, respectively, for all simulations across heating and cooling modes. To ensure a consistent system charge independent of the enthalpy or temperatures inside the VCC loop, a controller for system charge is introduced. This controller acts as a point source or sink where refrigerant mass can enter or exit the system. For the purposes of this simulation the system charge is set to 0.75 kg. The thermal masses throughout the system include the battery, power electronics, cabin component, heat exchangers, and the various fluids (water/glycol, mixed air, refrigerant). A soak initialization condition is chosen such that the thermal masses inside of the system are initialized at the ambient temperature for the test condition. The battery is initially charged to SOC = 0.95 with an initial current of zero. For the water glycol circulating loops the PI controls are initialized at 0.25 kg/s while the compressor and mass flow through the VCC system are initially shutoff.

4.3 Simulation cases

The simulated conditions sweep across a range of ambient temperatures, cabin set point temperatures. Battery setpoint temperatures following logical temperatures in heat and cooling modes were also initially investigated, but they caused no appreciable difference on system range. Test cases are performed at fixed ambient temperatures of -20 °C, -10 °C, 0 °C, 10 °C, 25 °C, 30 °C, and 40 °C. At each ambient temperature, the cabin setpoint is evaluated at 18 °C, 20 °C, 22 °C, and 24 °C. The cabin setpoints determine the heating or cooling targets of the system across the simulated MCT cycle. All of the ITMS architectures are evaluated across all setpoint combinations; cases where specific system architectures fail to achieve these targets are discussed

in the results. The achievable driving range and transient performance is compared across each system architecture for cases where the setpoints can be achieved. During heating simulation cases the battery setpoint is 15 °C and during cooling cases the battery is set to 35 °C.

5. Results

With the modeling methodology, thermal system architectures, and boundary conditions established, the six thermal management systems are simulated across the MCT cycle. This allows for comparisons of driving range across parameters of the thermal management system, ambient temperature, and cabin setpoint temperature. Finally, a transient cycle for the WHR system of most interest is examined across a MCT simulation, highlighting the heat transfer and control setpoints during transient performance.

5.1 Comparison of Driving Ranges

The bar charts presented in Figure 3 show the system ranges across the range of ambient temperatures at each cabin setpoint temperature. Battery trials are excluded as their results had little impact on overall system range varying the overall range approximately 2% across the investigated range of battery variation. Clear trends are observed in system performance as the cabin setpoint varies across the range of ambient temperatures. On average, for each architecture in most stringent cooling mode (i.e., ambient temperature of 40 °C). the projected range for the system decreases by approximately 2-3% for every 2 °C reduction in the cabin setpoint from 24 °C to 18 °C. This leads to an overall variation of 12% in driving range for the baseline system depending on the user-determined cabin set point. These cycles have the same cooling performance, except the LT HX system, because all of their assumed components and control behavior are identical in cooling mode.
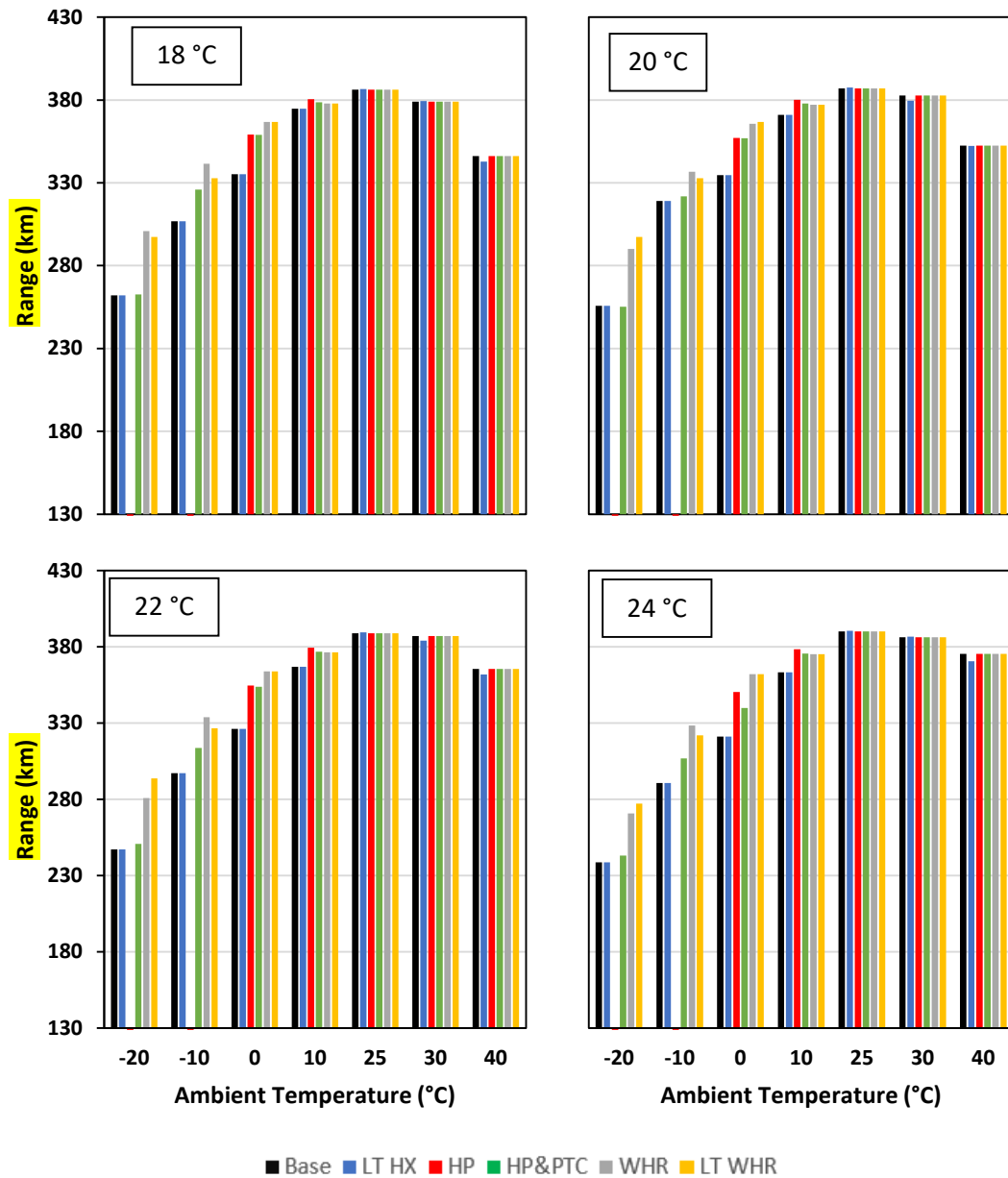
Figure 3: Simulated driving ranges for each ITMS architecture (Base, LT HX, HP, HP&PTC, WHR, and LT WHR) across a parametric variation in ambient temperature (-20 °C, -10 °C, 0 °C, 10 °C, 25 °C, and 30 °C) at cabin setpoints of: a. 18 °C, b. 20 °C, c. 22 °C, and d. 24 °C.

The LT HX system was theorized to provide low temperature cooling for the battery, but compared to the baseline, provides only a very slight benefits at the 25 °C ambient condition, while showing no benefit at the other test conditions. This radiator, while implemented to provide low

temperature cooling of the battery, was observed to only provide benefit in a mixed heating and cooling condition, namely, when the cabin requires marginal heating while the battery would require cooling. The range of ambient conditions tested does not provide many opportunities for this necessary mixed condition where cabin conditioning would be negligible, and the battery could be cooled with a relatively cool ambient. Future work could examine a mix of moderate test conditions to examine mixed system use-cases that might highlight the benefits of this system.

Under the ambient temperature range that demands cabin heating (from -20 °C to 10 °C), the system architectures become more distinct in their performance. Compared to the cooling demands, these heating cases have more severe impact on driving range that justifies our focus on exploring architecture improvements for heating efficiency. Beginning with a general assessment, an overall decrease in the max range of 32.9% to 38.9%, depending on the cabin setpoint temperature, is experienced by the baseline system as the ambient temperature is reduced to -20 °C. This amounts to a total range reduction of 80 to 100 miles for the baseline system. Examining the heat pump architecture (HP), improved performance relative to the baseline is observed at ambient temperatures ranging from 0 °C to 10 °C, but the heating performance is inadequate to meet the heating demand at -20 °C and -10 °C (bars therefore not shown for these unviable operating points). There are several potential solutions to this issue with the HP system. Active control of the recirculation ratio could decrease the ventilation loading and allow for adequate heating of the cabin down to low ambient temperatures of -20 °C; however, this would risk fogging of the windshield and pose a hazard to driver safety. Alternatively, the compressor size (which was sized for the baseline system cooling load) could be increased to provide the necessary capacity at lower ambient temperatures, with the tradeoffs being additional cost, size, and weight of the VCC components. Finally, the addition of an electric heater to compensate for

lack of capacity is the most practical solution, and the basis for the HP&PTC architecture. This HP&PTC architecture maintain the performance gains of the HP system relative to the baseline at ambient temperatures of 0 °C to 10 °C. More critically, the addition of the PTC heater makes up any heating capacity shortfalls of the heat pump system, but compared to the baseline, the continued operation of the compressor at low temperature benefits the system it can provide heating with a COP > 1. Ultimately, this HP&PTC architecture can achieve the cabin setpoints at -20 °C (with little range benefit) and provides a measurable range increase of ~5% over the baseline system at -10 °C. This extends the use of a traditional HP scheme to a lower temperature bound and maintains the HP performance improvements at moderate temperatures of 0 °C to 10 °C with this simple addition of a four-way valve (V4).

With the baseline system's use of water glycol loops for cabin and battery conditioning, the WHR architecture was established to allow heat scavenging from the electronics cooling loop. The WHR system mirrors the range performance of the HP&PTC system at moderate ambient temperatures, but provides clear advantages at lower ambient temperatures (0 °C to -20 °C). At these temperatures, the system experiences a further increase in effective range owing to the utilization of waste heat. At the 0 °C ambient condition, only a moderate increase of 3% in driving range is gained as compared to the HP&PTC system because the system load can still be met with the compressor. But at the -10 °C and -20 °C test conditions, the compressor cannot provide all of the heating load necessary for the cabin in the HP&PTC system. At these ambient temperatures, the WHR system can supplement the necessary cabin heating requirements, which leads to a 13.5% relative increase in range as compared to the baseline system. This increase is largest at the -20 °C condition as a larger portion of electric heating is needed to meet the demand in the HP&PTC system compared to the WHR system. The next section will further discuss the transient response

of the WHR system to illustrate the reduced electric heating load due to recovered heat from the power electronics.

Further improvements to the extreme low temperature performance motivated the analysis of the LT-WHR architecture. With the addition of the low temperature battery radiator in this system, the results at -20 °C ambient are investigated and compared to the WHR system to determine if the LT waste heat utilized by the LT WHR system provides a significant benefit to system range. As observed in Figure 3, this depends upon the cabin setpoint temperature. At - 20 °C, with a cabin setpoint of 20 °C to 24 °C the LT-WHR system provides an appreciable increase in system range of 2% compared to the WHR architecture. At an 18 °C cabin setpoint and -20 °C ambient there appears to a penalty imposed by this system. This is due to oscillation of the electric PTC heater as it nears its shutoff condition. This prolongs the use of this heater and causes the decrease in range observed. This performance benefit observed at setpoints of 20 °C to 24 °C cabin setpoints disappears however at any higher ambient temperatures because the recovered heat from the power electronics is sufficient to supplement the steady state electric heating requirements of the system. The addition of the low temperature radiator in the LT-WHR system has no performance benefit as the offset compressor power is already negligible at this point. Overall, the implementation of this LT-WHR system, while it provides for increased system range at extremely low ambient temperatures, provides little overall benefit for the increase in complexity and necessary system components.

Considering the tradeoffs in system complexity versus range benefits over a wide range of typical ambient and cabin temperature, the WHR system seems to be optimal ITMS for long range electric vehicles among the architectures compared in this study. A logical extension of this modeling work is an addition to the modeling framework for technoeconomic investigation of the

systems to quantify their range extension in terms of added system components and complexity. This could allow broad comparison of the technoeconomic tradeoffs between candidate EV thermal systems.

5.2 Transient ITMS response

Shown in Figure 4 is a plot of the transient compressor power, PTC heater power, and cabin HX throughout the drive cycle for the WHR architecture simulated at an ambient temperature of -10 °C, a cabin setpoint of 24 °C, and a battery setpoint of 15 °C. Several features of the control logic are illustrated in this plot. First, from the initialized soak condition, the electric heater for the cabin is set to a maximum of 6 kW of power, in contrast with that of the HP&PTC architecture that necessitated an 8 kW maximum (not shown). This is due to the added waste heat in the system as well as the battery and cabin heater being placed in line with each other, allowing them to work together in heating operation. A clear gap in heating performance is observed between 0 s and when the cabin then reaches its setpoint at ~1400 s. The 6 kW of power for the electric heater appears to not be transferred to the cabin HX. This is due to the orientation and layout of the flow control systems in the WHR architecture, the thermal mass of the battery, and the size of the battery heater itself. Its observed from Figure 2e that the cabin PTC heater flows into the battery which extracts heat before the cabin HX, effectively delaying the heating action of the cabin which can be seen completes at 1400 s in the transient plot, at which point the PTC heater begins to adjust to control the inlet cabin temperature while the system actuates the inlet volume flow rate. A corresponding dip in battery heating can be observed. In this way, the sizing of the battery heater, the orientation of the flow systems, and the battery thermal mass can have significant deleterious effects on the cabin heating performance which are clearly demonstrated.
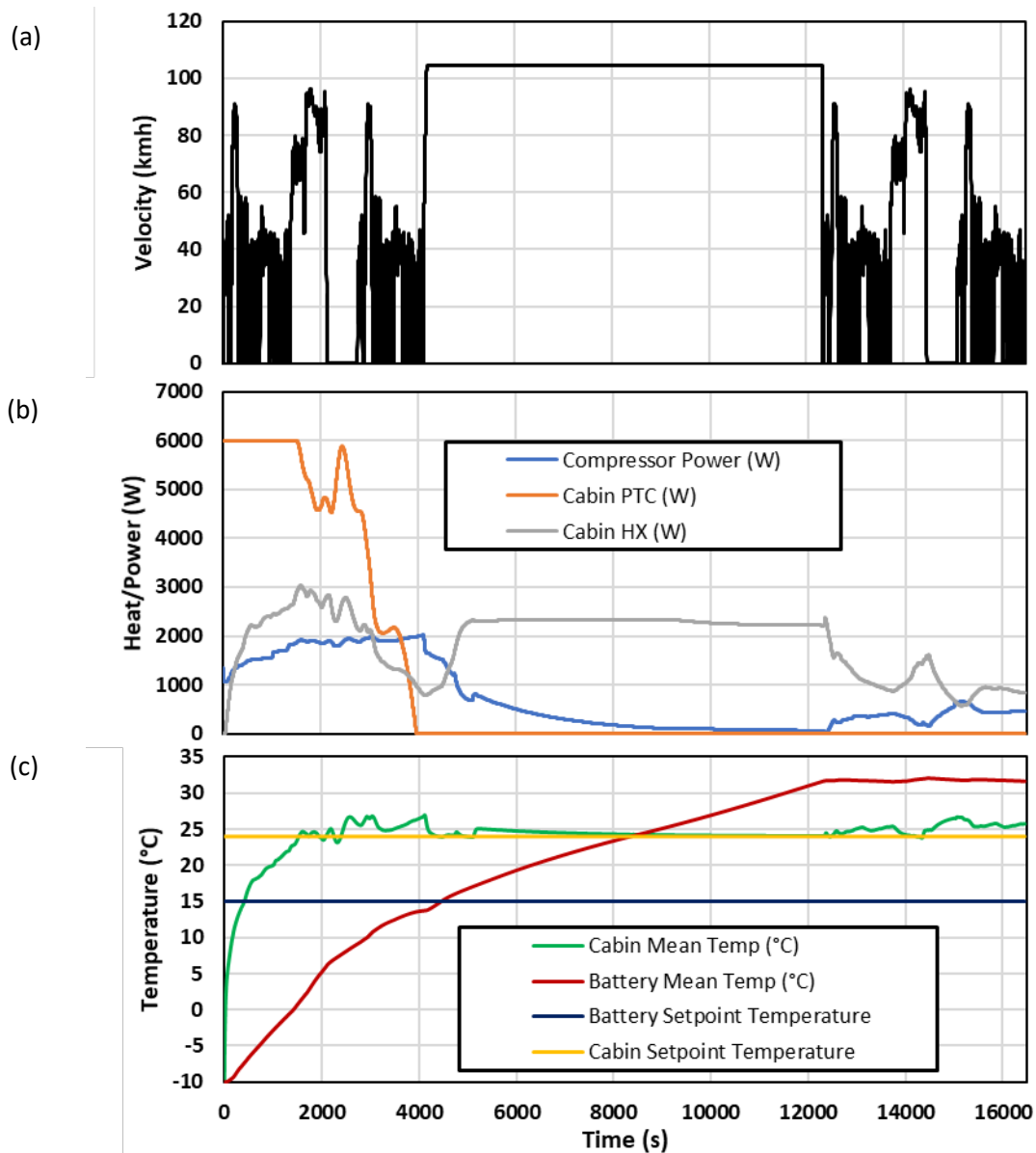
Figure 4: (a) simulated MCT drive cycle. The simulated heat loads and power draws throughout the cycle time are plotted for: (b) the heat exchange in the WHR architecture at -10 °C ambient with a 24 °C cabin and 15 °C battery setpoints; and (c) the setpoints of the WHR architecture at -20 °C ambient with a 24 °C cabin and 15 °C battery setpoints

At this point, from 1700 s to 2600 s, the flow rate into the system initially decreases as the cabin setpoint is surpassed and, due to slight fluctuations in PI control, dips briefly below its setpoint until settling at the control point as the fan volume flow rate decreases. Eventually, at

~4000 s, the electric heater completely shuts off while the cabin HX and compressor power completely compensate for the necessary steady state heating load of the system. As time progresses, during the high constant speed portion of the cycle, the WHR supplements most of the heating load, allowing the compressor to essentially shut off. After this constant speed portion, at ~12000 s, the system enters a mixed control condition where the compressor controls the cabin inlet temperature while the power electronics radiator is completely bypassed. Overall, this control scheme and architecture meets the necessary EV setpoint temperatures while extending system range via the utilization of waste heat. Compared to the baseline, this flow control is enabled through the addition of a four-way valve (V4) to allow operation of the VCC as a heat pump and two four-way valves (V5 and V6) actuated to allow waste heat recovery. Implications on future work and system implementation are clear, as this result demonstrates the need for study on effective and flexible flow configuration, as well as the benefits of battery and cabin pre-heating.

6. Conclusion

This work performed a comparative investigation of integrated thermal management systems (ITMS) for long-range battery electric vehicles, using a comprehensive dynamic model to evaluate the range performance across various thermal systems architectures. This is completed for traditional thermal management systems commonly studied in open literature as well as a novel solution defined for this work. This approach unifies results that were previously scattered across a wide range of boundary conditions, vehicle drive schedules, and user-defined control parameters, hampering a direct comparative analysis. The impacts on range of cabin thermal management are clearly enumerated with the impacts of the large thermal masses of the battery and cabin quantified in a transient simulation of mixed control schemes. These have broad implications for the optimal thermal management system for long-range EV's.

Several key conclusions are drawn regarding long-range BEV thermal system performance:

- First, from the HP&PTC architecture, the extension of system heating performance with a PTC heater can yield extended range, up to a 5% increase, above the baseline system even at extremely low ambient temperatures of -10 °C.

- Second, the inclusion of the battery as a necessary heating mass requires the cabin electric heater to be increased in size, up to 9 kW, and delays cabin conditioning in a WHR scenario up to 1400 s into the drive cycle.

- Third, the advantages of the WHR system is further shown when examining the components necessary to enable its advantages; namely only the addition of three four-way, flow reversing valves and the use of a common heat transfer fluid, water glycol.

- Fourth, the novel LT WHR system defined in this work, provides some performance benefit compared to a WHR system, a 2% range increase at -20 °C, but not enough to justify the additional equipment and control structures necessary.

- Fifth, a comprehensive review of battery circuit modeling is conducted with the perspective of integration of open source data with flexible modeling platforms. It was concluded that usable, temperature-based, ECM's are rare in literature and should be examined in the future.

- Finally, WHR systems provide unique benefits, up to 13.5% added range, for long-range systems operating over long range cycles at extremely low ambient temperatures.

Natural extensions of this work could be the adoption of additional novel thermal management systems such as direct two-phase cooling of the battery, investigations into gain scheduling, battery and cabin pre-heating control schemes, and charging scenarios and associated battery thermal management.

References

[1] J. Kim, J. Oh and H. Lee, "Review on battery thermal management system for electric vehicles," *Applied Thermal Engineering,* vol. 149, pp. 192-212, 2018.

[2] M. Al-Zareer, I. Dincer and M. A. Rosen, "A review of novel thermal management systems for batteries," *International Journal of Energy Research,* vol. 42, no. 10, pp. 3182-3205, 2018.

[3] Y. Deng, C. Feng, J. E, H. Zhu, J. Chen, M. Wen and H. Yin, "Effects of different coolants and cooling strategies on the cooling performance of the power lithium ion battery system: A review," *Applied Thermal Engineering,* vol. 142, pp. 10-29, 2018.

[4] A. Tang, J. Li, L. Lou, C. Shan and X. Yuan, "Optimization design and numerical study on water cooling structure for power lithium battery pack," *Applied Thermal Engineering,* vol. 159, p. 113760, 2019.

[5] Z. An, K. Shah, L. Jia and Y. Ma, "A parametric study for optimization of minichannel based battery thermal," *Applied Thermal Engineering,* vol. 154, pp. 593-601, 2019.

[6] X. Li, D. Zhou, G. Zhang, C. Wang, R. Lin and Z. Zhong, "Experimental investigation of the thermal performance of silicon cold plate for battery thermal management system," *Applied Thermal Engineering,* vol. 155, pp. 331-340, 2019.

[7] Z. Zhang, J. Wang, X. Feng, L. Chang, Y. Chen and X. Wang, "The solutions to electric vehicle air conditioning systems: A review," *Renewable and Sustainable Energy Reviews,* vol. 91, pp. 443-463, 2018.

[8] G. Titov and J. Lustbader, "Modeling control strategies and range impacts for electric vehicle integrated thermal management systems with MATLAB/Simulink," *SAE Technical Paper,* no. 2017-01-0191, 2017.

[9] A. Carriero, M. Locatelli, K. Ramakrishnan, G. Mastinu and M. Gobbi, "A review of the state of the art of electric traction motors cooling techniques," *SAE Technical Paper,* no. 2018-01-0057, 2018.

[10] K. J. Kelly, T. Abraham, K. Bennion, D. Bharathan, S. Narumanchi and M. O'Keefe, "Assessment of thermal control technologies for cooling electric vehicle power electronics," in *23rd International Electric Vehicle Symposium (EVS-23)*, Anaheim, 2007.

[11] A. Bhunia, S. Chandrasekaran and C.-L. Chen, "Performance improvement of a power conversion module by liquid micro-jet impingement cooling," *IEEE Transactions on Components and Packaging Technologies,* vol. 30, no. 3, pp. 309-316, 2007.

[12] B. Yu, J. Yang, D. Wang, J. Shi and J. Chen, "Energy consumption and increased EV range evaluation through heat pump scenarios and low GWP refrigerants in the new test procedure WLTP," *International Journal of Refrigeration,* vol. 100, pp. 284-294, 2019.

[13] Z. Wang, M. Wei, F. Peng, H. Liu, C. Guo and G. Tian, "Experimental evaluation of an integrated electric vehicle AC/HP system operating with R134a and R407C," *Applied Thermal Engineering,* vol. 100, pp. 1179-1188, 2016.

[14] Z. Tian, W. Gan, X. Zhanga, B. Gub and L. Yang, "Investigation on an integrated thermal management system with battery cooling and motor waste heat recovery for electric vehicle," *Applied Thermal Engineering,* vol. 136, pp. 16-27, 2018.

[15] Z. Zhang, W. Li, C. Zhang and J. Chen, "Climate control loads prediction of electric vehicles," *Applied Thermal Engineering,* vol. 110, pp. 1183-1188, 2017.

[16] T. J. Shelly, J. A. Weibel, D. Ziviani and E. A. Groll, "A Dynamic Simulation Framework for the Analysis of Battery Electric Vehicle Thermal Management Systems," in *19th IEEE Intersociety Conference on Thermal and Thermomechanical Phenomena in Electronic Systems (ITherm)*, Orlando, 2020.

[17] Dassault Systèmes, "What is Dymola?," Dassault Systèmes, Boston , 2019.

[18] TLK-Thermo GmbH, "TIL Suite," August 2020. [Online]. Available: https://www.tlk-thermo.com/images/tlk/content/presentations/TIL_Suite_EN_2020_August.pdf. [Accessed 21 July 2021].

[19] L. Lam, P. Bauer and E. Kelder, "A practical circuit-based model for Li-ion battery cells in electric vehicle applications," in *IEEE 33rd International Telecommunications Energy Conference (INTELEC)*, Amsterdam, 2011.

[20] J. Jaguemont, L. Boulon and Y. Dubé, "Characterization and Modeling of a Hybrid-Electric-Vehicle Lithium-Ion Battery Pack at Low Temperatures," *IEEE Transactions on Vehicular Technology,* vol. 65, no. 1, pp. 1-14, 2015.

[21] Y. Tripathy, A. Mcgordon and C. Low, "A New Consideration for Validating Battery Performance at Low Ambient Temperatures," *Energies,* vol. 11, no. 9, p. 2439, 2018.

[22] T. Huria, M. Ceraolo, J. Gazzarri and R. Jackey, "High fidelity electrical model with thermal dependence for characterization and simulation of high power lithium battery cells," in *IEEE International Electric Vehicle Conference*, Greenville, 2012.

[23] D. Cittanti, A. Ferraris, A. Airale, S. Fiorot, S. Scavuzzo and M. Carello, "Modeling Li-ion batteries for automotive application: A trade-off between accuracy and complexity," in *International Conference of Electrical and Electronic Technologies for Automotive*, Torino, 2017.

[24] S. Arianto, R. Y. Yuwono and B. Prihandoko, "Modeling of Lithium Ion Battery Using Modelica and Scilab/Xcos," in *ECS Transactions*, San Diego, 2016.

[25] A. Nikolian, J. Jaguemont, J. D. Hoog, S. Goutam, N. Omar, P. V. D. Bossche and J. V. Mierlo, "Complete cell-level lithium-ion electrical ECM model for different chemistries (NMC, LFP, LTO) and temperatures (−5 °C to 45 °C) – Optimized modelling techniques," *International Journal of Electrical Power & Energy Systems,* vol. 98, pp. 133-146, 2018.

[26] A. Fotouhi, S. Longo, D. Auger and K. Propp, "Electric Vehicle Battery Parameter Identification and SOC Observability Analysis: NiMH and Li-S Case Studies," in *8th IET International Conference on Power Electronics, Machines and Drives*, Glasgow, 2016.

[27] Y. Chen, Y. Ma, P. Duan and H. Chen, "Estimation of State of Charge for Lithium-ion Battery Considering Effect of Aging and Temperature," in *Chinese Control Conference*, Wuhan, 2018.

[28] Z. Yang, D. Patil and B. Fahimi, "Electrothermal Modeling of Lithium-Ion Batteries for Electric Vehicles," *IEEE Transactions on Vehicular Technology,* vol. 68, no. 1, pp. 170-179, 2019.

[29] M. Bahramipanah, D. Torregrossa, R. Cherkaoui and M. Paolone, "Enhanced Equivalent Electrical Circuit Model of Lithium-Based Batteries Accounting for Charge Redistribution, State-of-Health, and Temperature Effects," *IEEE Transactions on Transportation Electrification,* vol. 3, no. 3, pp. 589-599, 2017.

[30] N. A. Samad, J. B. Siegel and A. G. Stefanopoulou, "Parameterization and Validation of a Distributed Coupled Electro-Thermal Model for Prismatic Cells," in *ASME 2014 Dynamic Systems and Control Conference* , San Antonio, 2015.

[31] M. Yazdanpour, P. Taheri, A. Mansouri and B. Schweitzer, "A circuit-based approach for electro-thermal modeling of lithium-ion batteries," in *32nd Thermal Measurement, Modeling & Management Symposium (SEMI-THERM)*, San Jose, 2016.

[32] A. I. Stroe, D. I. Stroe, M. Swierczynski, R. Teodorescu and S. K. Kær, "Lithium-ion battery dynamic model for wide range of operating conditions," in *International Conference on Optimization of Electrical and Electronic Equipment (OPTIM) & 2017 Intl Aegean Conference on Electrical Machines and Power Electronics (ACEMP)*, Brasov, 2017.

[33] K. Li, F. Wei, K. J. Tseng and B.-H. Soong, "A Practical Lithium-Ion Battery Model for State of Energy and Voltage Responses Prediction Incorporating Temperature and Ageing Effects," *IEEE Transactions on Industrial Electronics,* vol. 65, no. 8, pp. 6696-6708, 2018.

[34] A. Mevawalla, S. Panchal, M. Tran, M. Fowler and R. Fraser, "One dimensional fast computational partial differential model for heat transfer in lithium-ion batteries," *Jounral of Energy Storage,* vol. 37, p. 102471, 2021.

[35] S. Panchal, J. McGrory, J. Kong, I. Dincer, M. Agelin-Chaab, R. Fraser and M. Fowler, "Cycling degradation testing and analysis of a LiFePO4 battery at actual conditions," *International Journal of Energy Research,* vol. 41, no. 15, pp. 2565-2575, 2017.

[36] AHRI, "Performance Rating of Positive Displacement Refrigerant Compressors," Air-Conditioning, Heating, & Refrigeration Institute, Arlington, 2020.

[37] A. Dabiri and C. Rice, "A compressor simulation model with correction for the level of suction gas superheat," *ASHRAE Transactions,* vol. 87, no. 2, pp. 771-782, 1981.

[38] F. Nielsen, S. Gullman, F. Wallin, Å. Uddheim and J.-O. Dalenbäck, "Simulation of Energy Used for Vehicle Interior Climate,," *SAE International Journal of Passenger Cars and Mechancial Systems,* vol. 8, no. 4, pp. 1218-1234, 2015.

[39] SAE, "Surface vehicle reccomended practice: Battery Electric Vehicle Energy Consumption and Range Test Procedure," SAE International, Evanston, 2017.

[40] S. E. Mattsson and H. Elmqvist, "Modelica - An International Effort to Design the Next Generation Modeling Language," *IFAC Proceedings Volumes,* vol. 30, no. 4, pp. 151-155, 1997.